

Performance Evaluation of a Prognostic Framework for Electro-Hydraulic Actuators for Stability Control Augmentation Systems with Different Sensors Suites

Original

Performance Evaluation of a Prognostic Framework for Electro-Hydraulic Actuators for Stability Control Augmentation Systems with Different Sensors Suites / De Martin, A.; Jacazio, G.; Sorli, M.. - 14:(2022). (Intervento presentato al convegno 2022 Annual Conference of the Prognostics and Health Management Society, PHM 2022 tenutosi a Nashville, TN (USA) nel 2022) [10.36001/phmconf.2022.v14i1.3289].

Availability:

This version is available at: 11583/2978194 since: 2023-04-27T12:37:38Z

Publisher:

Prognostics and Health Management Society

Published

DOI:10.36001/phmconf.2022.v14i1.3289

Terms of use:

This article is made available under terms and conditions as specified in the corresponding bibliographic description in the repository

Publisher copyright

(Article begins on next page)

Performance Evaluation of a Prognostic Framework for Electro-Hydraulic Actuators for Stability Control Augmentation Systems with Different Sensors Suites

Andrea De Martin¹, Giovanni Jacazio², and Massimo Sorli³

^{1,2,3}*Department of Mechanical and Aerospace Engineering, Politecnico di Torino, Torino, 10129, Italy*

andrea.demartin@polito.it

giovanni.jacazio@formerfaculty.polito.it

massimo.sorli@polito.it

ABSTRACT

Stability Control Augmentation Systems (SCAS) are widely adopted to enhance the flight stability of rotary-wing aircraft operating in difficult aerodynamic conditions, such as low altitude missions, stationary flight nearby vertical walls or in presence of heavy gusts. Such systems are based upon small electro-hydraulic servosystems controlled in position through a dedicated servovalve. The SCAS operates with limited authority over the main control linkage translating the pilot input in the movement of the main flight control actuator. Being critical for the operability of the helicopter, the definition of a Prognostics and Health Management (PHM) framework for the SCAS systems would provide significant advantages, such as better risk mitigation, improved availability, and a reduction in the occurrences of unpredicted failures which still represent one of the most known downsides of helicopters due to their very severe operational environment. Since SCAS actuators are usually equipped with a low number of sensors, it is at the present time unclear whether a fully realized PHM system can be prepared without resorting to the introduction of additional sensors. This paper deals with this subject evaluating the performances of a fault diagnosis tool operating considering different sensors suite (traditional and with additional sensors), and different PHM strategies, using in-flight data or their combination with dedicated pre-flight checks to cover the most common failure modes. The analysis is then completed with an evaluation of the prognostic capabilities of the proposed strategies, highlighting benefits and limitations of the proposed solutions.

Keywords: PHM, Prognostics, Diagnostics, SCAS, Actuator, Servovalve, hydraulic actuator

Andrea De Martin et al. This is an open-access article distributed under the terms of the Creative Commons Attribution 3.0 United States License, which permits unrestricted use, distribution, and reproduction in any medium, provided the original author and source are credited.

1. INTRODUCTION

Stability Control Augmentation Systems are widely adopted in the flight controls of rotary wing aircraft to enhance the vehicle stability in difficult aerodynamic conditions, such as low altitude missions, stationary flight nearby vertical walls or in presence of heavy gusts. SCAS systems are based upon small electro-hydraulic position-controlled servosystems on the command linkage mechanism of the flight control actuator. Due to their short stroke and responding to safety concerns, SCAS actuators have a limited authority over the movement of the main actuator. Being critical for the operability of the helicopter, the definition of a Prognostics and Health Management framework would provide significant advantages to the users, such as better risk mitigation, improved availability, and a reduction in the occurrences of unpredicted failures which still represent one of the most known downsides of helicopters. A preliminary analysis on the effects of the inception and progression of several degradation types is the first step towards assessing if such PHM system is feasible, and which failure modes are more likely to be observed.

Authors already investigated the effects of several faults mode on electro-hydraulic servo actuators (EHSA) through theoretical (Autin et al., 2018) and experimental (Autin et al., 2020; Bertolino et al., 2021) activities for fixed wing aircraft, addressing the feasibility of the definition of a dedicated PHM system without resorting to additional sensors. Literature on prognostics for EHSAs is so far limited, and mostly focused on a few single faults scenarios; in (Byington et al., 2004), authors presented one of the few research papers focused on the hydraulic actuators for aviation. The authors examine the possibility of developing a PHM system for the F/A-18 stabilizer Electro-Hydraulic Servo-Valves (EHSV). The data-driven approach developed uses neural network error-tracking techniques, along with fuzzy logic classifiers, Kalman filter state predictors, and feature fusion strategies. In (Guo & Sui, 2019) authors proposed a new resampling

scheme based on Hellinger's distance and verified their results on accelerated fatigue tests on a few structural components of the actuator, while a fault diagnosis scheme for electro-hydrostatic actuation system is briefly described in (Chen et al., 2019).

Results of these research activities are promising but not directly applicable to the case of the SCAS actuators; these devices are in fact different in design and type of usage, while also lacking some signals instrumental to the observation of faults within EHSAs for other applications, thus making more difficult to extract features unique for each considered failure mode. SCAS actuators are not directly subjected to the aerodynamic load, and the only force disturbance acting on their control loop is due to the combined effect of a recentring spring, which is fundamental for the system safety, and friction. To pursue this analysis, a detailed model of the flight control actuator has been prepared and several significant failure modes investigated. For the servovalve, issues in the feedback spring (backlash and crack inception), in the torque motor (windings short and degradation of the permanent magnets) and in the jet-pipe (occlusion and deformation of the channel) were considered. For the actuator, wear of the dynamic seals, crack inception in the recentring spring, and a short within the coils of the Linear Variable Differential Transducer (LVDT) sensor are considered. Then, an in-depth simulation campaign was pursued with the aim of studying the interactions between different failure modes, the effects that the propagating degradations have on the system performances and which signals can be used to define a robust set of features.

The paper introduces the case-study under analysis, presenting the most prominent peculiarities of the system and the effect of such peculiarities on the definition of health monitoring schemes. Hence, the model used to describe the behaviour of the system under nominal and degraded conditions is introduced and the selected fault modes described with details. The results of a wide-ranging simulation campaign are then presented, where the time-domain response of the system is used to guide in the definition of a proper set of features able to characterize the selected fault cases. The paper builds on the preliminary study focused on a few selected fault cases (Nesci et al., 2020) and on the results of more extensive simulation activities (De Martin et al., 2021), which provided an early evaluation of a possible feature in function of the a few combinations of available sensors, either considering data obtained during simulated flight, during simulated pre-flight checks or their combination. Simulation results are then used to foster the definition of a fault diagnosis scheme operating under a few alternative assumptions considering different operational conditions (in-flight data, pre-flight data, both) and different sensors suit (typical configuration and in presence of dedicated sensors). Results are then presented and discussed, with the aim of providing early indications towards the definition of optimal PHM strategies for SCAS

actuators and lay the foundations for their verification through technological demonstrators.

2. CASE STUDY

The architecture of the case study under consideration is depicted in Figure 1, where one of the actuators controlling the collective and the cyclic pitch of the main rotor is represented. The pilot input acts on the upper segment of the main linkage, imposing the movement of the main control valve spool. The main control valve modulates the flow rate exchanged by each of the four chambers of the tandem hydraulic actuator with two independent hydraulic systems. The actuator's rod is connected through a spherical joint to the stationary swash plate.

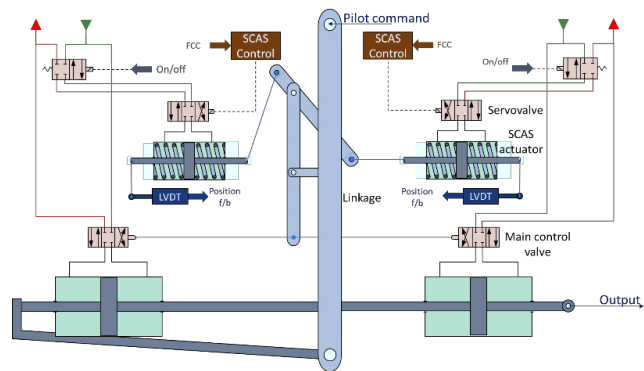


Figure 1. Case study

The position feedback of the hydraulic actuator is obtained through the motion of the main leverage, thus negating the need of a dedicated position sensor. Two SCAS systems, each based on a small electro-hydraulic servosystem, act on the linkage as well. The actuators of each SCAS system are supplied through two jet-pipe servovalves, while their position is monitored through two LVDT integral with their rod. The outputs of the position sensors are used to close the position control loop, which defines the voltage applied to the windings of the servovalves through a proportional-integrative law. The servovalve is of the jet-pipe type, and its torque motor is driven through two coils connected in parallel. Since the aerodynamic load acts on the main actuator, the rod of each SCAS system is only affected by the combined effect of the mechanical actions exerted by the two recentring springs and the friction forces provided by the sealing elements and the spherical joints. The SCAS actuator under consideration has a full stroke of ± 10 mm and is controlled through a 5 l/min servovalve. The system is supplied at a pressure ranging between 210 bar (at zero flowrate) and 195 bar (at full flow), while the return pressure is supposed to range between 1 bar and 7 bar. The system has a bandwidth of 3.5 Hz for set amplitudes equal to 30% of the half-stroke at nominal pressure, air fraction of 0.5% and oil temperature of 40°C.

2.1. Considered failure modes

Although the SCAS system is fairly simple it can be nonetheless subjected to a wide range of failure modes. According to specific guidelines for similar devices, the first step towards the definition of a PHM system for flight control actuators is the study of the failure modes possibly affecting the system through a dedicated Failure Mode, Effects and Criticality analysis (FMECA) aimed at prioritizing the most critical, frequent and observable degradations. Results of this operation pertaining to similar Electro-hydraulic servo-actuators are provided in (Autin et al., 2018), where a set of possible failure modes were identified as the most significant to define its health status. The same preliminary results of the FMECA analysis, and thus the failure modes to investigate, can be applied to the case study under analysis along with a few degradations typical of the SCAS actuators.

Looking at the servovalve, the following failure modes were addressed. The occurrence of a backlash between the feedback spring is a relatively frequent event which causes uncontrolled oscillations of the servovalve spool. In primary flight controls, it is often monitored by measuring the spool position through a dedicated LVDT sensor, which however is not traditionally present in SCAS systems. Another issue possibly affecting the feedback spring is the inception and propagation of a fatigue crack, which eventually evolves in the static failure of the component and the consequent loss of the SCAS system. Remaining within the first stage of the servovalve, a few key failure modes can affect the torque motor. The occurrence of a short in its windings can occur due to the natural, thermally driven degradation of the insulating materials, eventually accelerated by the ingress of foreign material. Other processes eventually affecting the behaviour of the first stage are the degradation of the permanent magnets and the alteration of the magnetic circuit due to the accumulation of particles within its gaps. The first is due to the well-reported ageing phenomenon, which is primarily driven by the repeated variation of the magnetic loading, temperature variations and the application of mechanical stresses (Nunes et al., 2020). The second fault mode can quickly degrade the performance of the system, but it is unlikely to be an on-going, slowly evolving process, thus making it not predictable and hence not suitable for PHM. Similar considerations can be provided for the occlusion of the jet-pipe channel due to debris within the hydraulic circuit. The deformation of the jet-pipe anchor is instead considered since an asymmetric behaviour of the first stage of the servovalve is the primary cause of the generation of null-bias currents, which is the most common failure mode these devices when employed in flight control systems.

Switching the focus to the actuator, the first degradation mode considered in this analysis is the wear of the dynamic seals, which naturally occurs due to adhesive and abrasive phenomena and cause the progressive increase of the flowrate lost due to internal leakages (Stachowiak & Batchelor, 2014). As already noted, each SCAS actuator is equipped with two

recentring springs; as for the elastic element within the servovalve, fatigue cracks can originate due the repeated mechanical stresses associated with a high number of operating cycles. Finally, electrical issues can arise in the position sensor.

2.2. Discussion on the available signals

To pursue the definition of a dedicated PHM system it is paramount to check which of the signals useful to the description of the dynamics of the system are available and eventually which signals could be derived by fusing the available information or by adding dedicated sensors. The application discussed in (Autin et al., 2020) was equipped with a relatively high number of sensors, used to provide the feedback signals needed to close the control loops and to monitor the system behavior by detecting the occurrence of a set number of failures. As well depicted in Figure 2, the case study under consideration is traditionally equipped only with a position sensor of the LVDT type, integral with the actuator's rod and used to close the position control loop. The servovalve currents are also measured for control and monitoring purposes. As such, the minimum set of signals which can be considered available to provide PHM functionalities for the SCAS system is limited to these two measurements and the position command received from the Flight Control Computers.

A few additional information, such as the actuator speed, can be obtained by numerically differentiating the available signals with respect to the registered time stamps. To compare the results of this study with previous experiences and to best present the potential of a PHM system designed for SCAS actuators, a few additional sensors were considered as well. In particular, the possibility to add a position sensor on the servovalve spool and a differential pressure sensor on the actuator was evaluated. The measures provided by these additional sensors are then used in the feature selection process to assess the benefits of their presence and whether they are necessary or not.

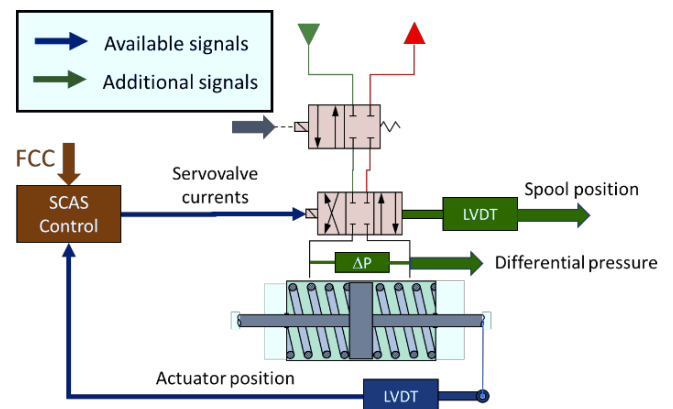


Figure 2. Schematics of a SCAS actuator

3. SIMULATION ACTIVITIES

Due to the lack of available data, especially regarding operations under faulty health conditions, a high-fidelity model of the SCAS actuator was prepared. Such model is presented in detail in (De Martin et al., 2021), where it was used to study the behavior of the system in nominal and off-nominal conditions, and hereby briefly introduced. It is worth reminding that although convenient, this approach alone could lead to misleading results without the support of an experimental validation. To limit this issue, the model was built using well-established equations available in literature which parameters are derived from the characteristic of currently in-service actuators. Previous experience on similar devices, complete with experimental evidence, was used as a further element to check the results of the simulations.

3.1. System modelling

The dynamic model of the system is based on the simulation environment for EHS defined and experimentally verified for nominal health conditions in (De Martin, Dellacasa, et al., 2018), where the servovalve physics is described according to the equations provided by Urata (Urata, 2007a, 2007b; Urata & Suzuki, 2011). This physics-based formulation allows to model the servovalve behavior without the introduction of linearized gains, requiring instead the accurate estimate of the device geometry and of the characteristics of its components. Although more complex, this approach allows to represent the faults possibly affecting the valve through physics-based models derived from literature, thus leading to more realistic results. The dynamics of the torque motor can be described as a sequence of an electric and a magnetic circuit, depicted in Figure 3 (a), and a mechanical equilibrium, represented in Figure 3 (b).

The resulting equilibrium equations provide a system of differential equation representing the physical interactions between each component of the servovalve first stage. V_S is the voltage applied to the servovalve windings, while i_1 and i_2 are the currents in each of the two parallel coils.

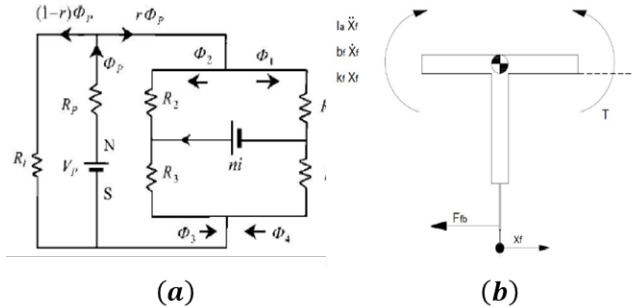


Figure 3. Magnetic circuit (a) and jet-pipe anchor (b) schematics

$$\begin{cases} V_S = [R_S(1 - W_S)]i_1 + L_S \frac{di_1}{dt} \\ V_S = R_S i_2 + L_S \frac{di_2}{dt} \\ T_m = T_m(\phi_p, i_1, i_2) \\ T_m - k_{jp}\vartheta_{jp} - k_{fb}[x_s - (y_{jp} + y_{dist})] + \\ -c\dot{\vartheta}_{jp} = I_{jp}\ddot{\vartheta}_{jp} \end{cases} \quad (1)$$

The occurrence of a short in one of the coils can be described reducing the winding resistance R_S of a value proportional to the damage extension W_S , while the winding inductance L_S can be in first approximation considered constant.

The torque T_m exerted by the torque motor can be described as a function of the magnetic flux generated by the permanent magnets ϕ_p , the servovalve currents i_1 and i_2 and the size of four gaps within the magnetic circuit. Consequently, the degradation of the permanent magnets can be represented by a variation of the magnetic flux ϕ_p . The torque provided by the motor is then the input signal for the dynamic equilibrium of the jet-pipe, which rotation ϑ_{jp} is determined by the combined effect of the anchor stiffness k_{jp} , its damping coefficient c_{jp} and its moment of inertia I_{jp} . The feedback spring acts on the equilibrium through its stiffness $k_{fb} = k_{fb}(x_b, a_{fb})$, function of the backlash x_b and of the crack length a_{fb} . The dependency on the backlash is such to provide null values of stiffness whether the relative position of the servovalve spool and the jet-pipe channel is lower than x_b , while the dependency on the crack size is such to reduce the stiffness value according to the equations provided in (Autin et al., 2018). The eventual strain of the anchor structure is modelled as an offset y_{dist} affecting the position of the discharge orifice y_{jp} . The movement of the jet-pipe defines the pressure differential at the opposite sides of the servovalve spool ($p_{v1} - p_{v2}$) through the hydraulic amplifier reported in Figure 4. Its behavior depends on the geometry of the receiving ports, on the supply pressure p_s .

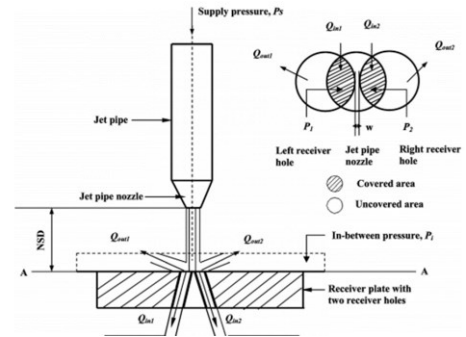


Figure 4. Schematics of the hydraulic amplifier

$$(p_{v1} - p_{v2})A_{sp} - k_{fb}(x_s - y_{jp}) - c\dot{x}_s - F_f + (-F_{fr,s} = m_s \ddot{x}_s) \quad (2)$$

The dynamics of the spool displacement x_s is described through Equation (2), where its dependency on the pressure drop across the control channels and on the force exerted by the feedback spring is reported. The friction force $F_{fr,s}$ acting in the contact points between the spool and the sleeve is modelled as a non-linear function to account for the stick/slip effect, while the flow force resultant $F_f = \sum_i \rho Q_i v_i \cos(\vartheta_i)$ is continuously computed as a function of the flowrates Q_1 and Q_2 exchanged with the actuator, the local speed of the fluid v_i and the expected flow deflection angle ϑ_i .

The flowrates Q_1 and Q_2 are computed according to the variable hydraulic resistances representing the metering section and the leakage path across the main stage of the servovalve. The dynamics of the SCAS actuator is instead represented through Equation (3), where the displacement of the rod x is obtained as a function of the pressure drop across the chambers ($p_1 - p_2$).

$$\begin{cases} Q_1 - A_c \dot{x} - Q_{l,i}(W_{w,i}) - Q_{l,e1}(W_{w,e1}) = \frac{V_0 + A_c x}{\beta} \frac{dp_1}{dt} \\ Q_2 + A_c \dot{x} + Q_{l,i}(W_{w,i}) - Q_{l,e2}(W_{w,e2}) = \frac{V_0 - A_c x}{\beta} \frac{dp_2}{dt} \\ (p_1 - p_2)A_c - [F_1^*(a_1) - F_2^*(a_2) + \dots \\ \dots + (k_1(a_1) + k_2(a_2))x] - F_{fr} - \gamma \dot{x} = m \ddot{x} \end{cases} \quad (3)$$

$Q_{l,i}$, $Q_{l,e1}$ and $Q_{l,e2}$ are the flow rates lost due to internal and external leakages. The trust areas of the two chambers are assumed equal to A_c , while the Bulk modulus and the chambers volume at mid stroke are addressed with β and V_0 . The flow-rate due to leakages are modelled according to a series of laminar and turbulent resistances, function of the amount of worn material W_w . The preload forces of the two recentering springs are identified as F_1^* and F_2^* , while their stiffness values are expressed as k_1 and k_2 . Both the preload and the stiffness values are dependent on the presence and size of cracks according to the equations provided in (Nesci et al., 2020). The friction forces due to the contact between the sealing elements and the components in relative motion are addressed with F_{fr} , while γ and m are respectively a viscous friction coefficient and the equivalent mass representative of the combined inertia of the rod and of the linkage.

3.2. Operational scenario

The definition of a realistic operational scenario is fundamental to obtaining meaningful results representative of real operating conditions. The SCAS system can operate in a wide range of environmental conditions and can be supplied with command of different shape, amplitude and frequency. The expected temperatures for the hydraulic fluid and the external environment, along with their probability of occurrence, are derived from previously published activities

(De Martin et al., 2020). Both the environmental conditions and the temperature of the hydraulic fluid influence several physical properties of the system and thus the associated parameters used within the model. As such, the fluid viscosity, density, and Bulk modulus are all expressed in function of the operating conditions, and the same happens for the friction parameters, and the mathematical expressions used to model the electro-magnetic behavior of the torque motor.

The model is then excited with a reference command signal defined by a sequence of a sinusoidal set with zero mean, a step, and a ramp (De Martin et al., 2021). This sequence was defined to meet two purposes. The first is to subject the actuator to different type of elementary shapes of command, each characterized by its own variance in amplitude and frequency rate. This operation is particularly important for the SCAS actuators since they are not subjected to the aerodynamic load and are thus more influenced by the non-linearities introduced by the friction forces. The second purpose is to mimic a possible command sequence that could be injected within the SCAS actuator during pre-flight or post-flight operations to extract a more refined set of features in more stable if not semi-controlled operating conditions to help the classification of the occurring faults. The use of a custom pre-flight sequence also provides the advantage of stressing the system in different operating points. The sinusoidal segment allows to easily observe and distinguish faults which affects the amplitude of the system response from those which primarily cause the generation of offsets in one or more measures. The step signal allows to study the system behavior close to the saturation limit associated with a full stroke of the servovalve spool. The ramp finally stresses the system at constant speed and, for the SCAS actuator, slowly rising load, which is the best operating condition to observe the occurrence of internal leakages. Simulations are then performed for both nominal health conditions and in presence of degradations.

Only one fault mode is active at any time, and the fault size is progressively increased up to failure conditions to study the system response in presence of different levels of degradation, where the ‘‘failure conditions’’ are defined as the health status of the system for which its performances are not acceptable (i.e., instability issues, excessive reduction of the servosystem bandwidth, loss of control, mechanical rupture). To quickly compare the results of simulations performed in presence of different degradations, we introduce the fault-ratio or fault severity as the ratio of the defect size against its critical value associated with the failure conditions. This number can range between 0 (completely healthy) and 1 (failed). An example of the simulation results is reported in Figure 5, where the behavior of the system in response to the pre-flight sequence for the case of crack propagation in one of the recentering springs is depicted. The SCAS actuator position x is barely affected by the propagating fault, and the same occurs for the servovalve currents i_s and the servovalve spool movement x_s . On the other hand, it is possible to

observe an increasing variation of the pressure drop ($p_1 - p_2$) across the actuator chambers, due to the effects of the stiffness reduction in one of the two springs on the rod equilibrium.

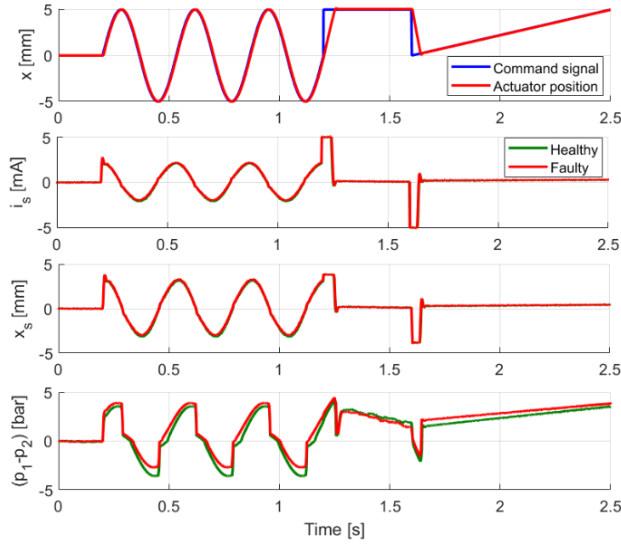


Figure 5. System behavior with a propagating crack in the recentering spring

4. FEATURE SELECTION

Feature selection is the process that aims to exploit a certain combination of signals to determine the best possible indexes associated with the fault modes under analysis among a pool of candidates. In principle, a feature suitable for the entire PHM process should exhibit a high correlation with the on-

going fault severity, a high value of signal-to-noise ratio, high accuracy and low dependency on all the other possible fault modes (Vachtsevanos et al., 2006).

To pursue this process, signals provided by the simulation environment were analyzed starting from the insight provided by previous studies (Autin et al., 2020). Several scenarios for feature selection were analyzed; the results, first provided in (De Martin et al., 2021), are hereby summarized for clarity. At first, in-flight data for the configuration complete with additional measures (servovalve spool position, differential pressure between the actuator’s chambers) were considered. Then, the same sensor suite was adopted for pre-flight checks. The results of these simulations were then analyzed combining only the traditionally available signals, both for the in-flight and pre-flight conditions, to check whether it is possible to extract meaningful information for the definition of a PHM system without additional sensors and eventually which operations could be performed. The behavior of the feature candidates computed in correspondence of actuator displacements higher than 3 mm is reported in Figure 6 (De Martin et al., 2021), where they are ranked according to the expected severity at detection, accuracy and correlation against the size of the associated fault. The radius of each data point is proportional to the signal-to-noise ratio. The optimal features are those that exhibits high correlation, low severity at detection, high accuracy and high signal-to-noise ratio. As such, the optimal choice of features considering the addition of dedicated sensors is the one reported in Table 1. Only a few of these features can be obtained without the need of additional sensors (SHSC2, JPDC3), while the degradation of the permanent magnets within the torque motor can be tracked even in-flight, although sub-optimally, via the index DTMC1.

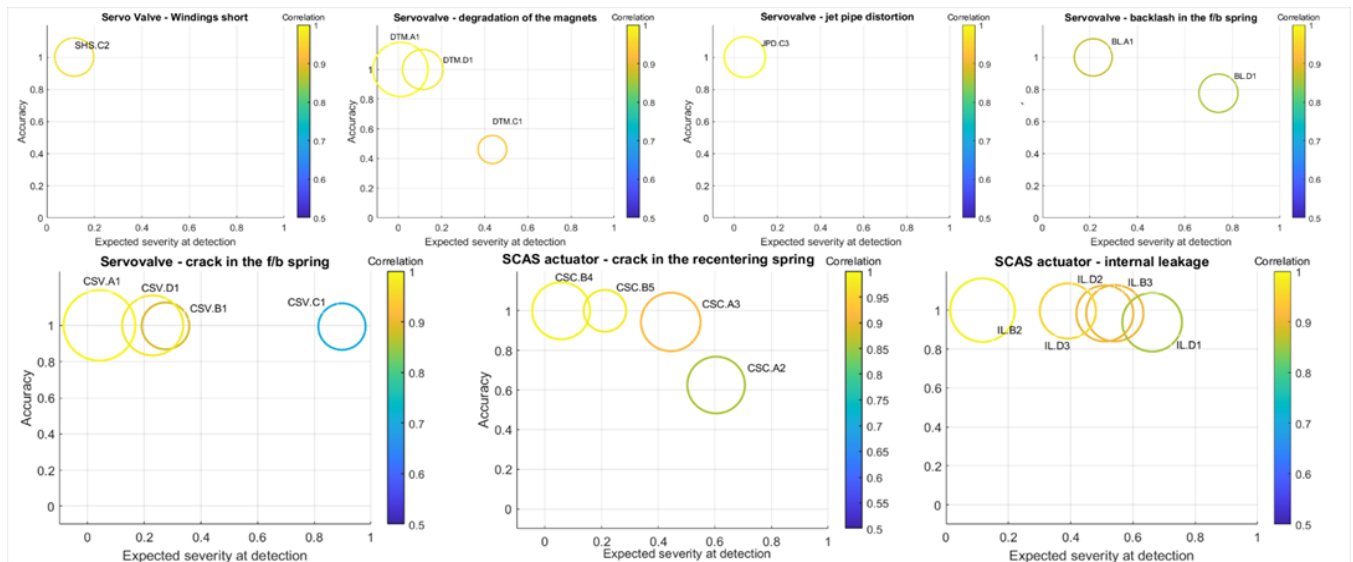


Figure 6. Performances of the feature candidates for each failure mode

More interesting results can be obtained focusing the attention on the candidates computed for the pre-flight checks. The index ILD3 scores high marks in all the considered metrics and seems suitable to detect the growth of internal leakages in the SCAS actuator through pre-flight checks. Similar considerations can be deduced from the behavior of the candidate DTMD1 for the degradation of the permanent magnets within the servovalve. The choice to focus at first only on conditions associated with relatively high-amplitude commands is due to the expected influence of the set signal on the possible feature candidates. For low set-amplitudes the dynamics of the SCAS actuator is more affected by non-linear phenomena such as friction and positive or negative overlaps in the servovalve, which can limit the effectiveness of the selected features. Moreover, the signal-to-noise ratio of real signals tends to decrease with their amplitude, hence increasing the relative uncertainty on the features making use of such measures.

Table 1. Optimal features set

| PRE-FLIGHT ONLY AND ADDITIONAL SENSORS | IN-FLIGHT AND ADDITIONAL SENSORS |
|---|--|
| SV: crack in the f/b spring (CSV.B1) A: crack in the recentering spring (CSC.B4) | SV: permanent magnets degradation (DTM.A1) SV: backlash in the f/b spring (BL.A1) SV: crack in the f/b spring (CSV.A1) A: crack in the recentering spring (CSC.A3) A: internal leakage (IL.B2) |
| PRE-FLIGHT ONLY AND NO ADDITIONAL SENSORS | IN-FLIGHT AND NO ADDITIONAL SENSORS |
| SV: permanent magnets degradation (DTM.D1) SV: backlash in the f/b spring (BL.D1) SV: crack in the f/b spring (CSV.D1) A: internal leakage (IL.D3) | SV: windings short (SHS.C2) SV: jet pipe distortion (JPD.C3) SV: permanent magnets degradation (DTM.C1) SV: crack in the f/b spring (CSV.C1) |
| Features encoding | |
| A1 = $\text{mean}(\frac{x_{sv}}{t_{com}})$ | C1 = $\text{mean}(\frac{x_{csc,a2}}{t_{com}})$ |
| A3 = $\text{mean}(x_{sv})$ | C2 = $\text{mean}(t_{com,1} - t_{com,2})$ |
| B1 = $\text{Std}(\frac{x_{sv}}{t_{com}})$ (step input) | C3 = $\text{mean}(t_{com})$ |
| B2 = $\text{mean}(\frac{x_{sv}}{p_1 - p_2})$ (ramp input and in-flight) | D1 = $\text{mean}(\frac{x_{csc,a2}}{t_{com}})$ (sinusoidal input) |
| B4 = $\text{mean}(p_1 - p_2)$ (sinusoidal input) | D3 = $\frac{c_{1,com}}{c_{2,com}}$ (ramp input) |

5. FAULT DIAGNOSIS

The fault diagnosis process is prepared as a succession of two subroutines, a purely data-driven fault detection algorithm followed by a classifier based on a Support Vector Machine. The fault detection algorithm continuously compares the running distribution of each considered feature against a baseline representing the feature behavior under healthy conditions. Such baseline is built in practice considering the SCAS behavior during its first flight hours. During operations, features are continuously computed and the new distribution compared to the initial baseline. When the running distribution differs from the baseline by a customizable confidence an alarm flag is raised. Such information is then sent, along with the feature vector, to the fault classification algorithm.

The fault classification is performed with a Linear Support Vector Machine, trained on simulated data-set and verified through a k-fold cross validation process (Anguita et al., 2012). The same combination of operational scenarios

and sensor suite used for the feature selection step were adopted and hereby presented. Confusion matrixes are presented according to two different conventions. Positive Predictive Values (PPV) against False Discovery Rates (FDR), used to better highlights the amount of false positive classification per predicted class, and True Positive Rate (TPR) against False Negative Rate (FNR), useful to quantify the success of the classifier in recognizing the on-going degradations and which other degradation is responsible for the misclassifications. Figures 7 and 8 depict the performances of the SVM trained and tested considering only in-flight data and without the presence of additional sensors. In this case, The SVM achieve a total accuracy score of 72.3 %. The following observation can be brought up. The degradation with the highest TPR and PPV is the short in the servovalve windings, which can be recognized through current asymmetry. The occurrence of a crack in the servovalve feedback spring (CSV) achieve good results for the TRP (88.4 %), but is often misclassified with the occurrence of a backlash between the spring and its seat (BL). The worst performances are achieved in presence of faults related to the actuator, with the internal leakage (LI) and the crack in the recentering spring (CSC) being mutually misclassified, highlighting the need of additional sensors or dedicated ground testing to be successfully identified.

It is worth noting however, that most of the misclassifications are associated with faults occurring in the same component (servovalve faults are rarely attributed to the hydraulic actuator and viceversa). As shown in Figure 9 and 10, the introduction of on-ground testing provides significant improvements to the classification performance. The SVM considering both in-flight and pre-flight data scores a total accuracy of 93.5 %. Although there is a noticeable improvement, classification issues remain in distinguishing between the occurrence of a backlash and a crack in the feedback spring, as well as between the occurrence of internal leakages and the cracking of the recentering spring in the actuator.

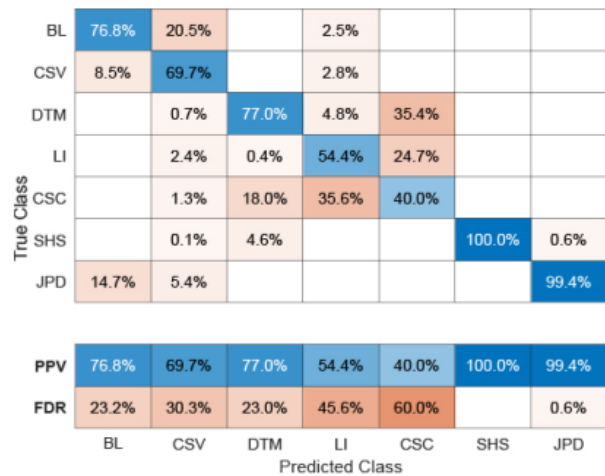


Figure 7. In-flight and pre-flight data – no additional sensors: PPV vs FDR

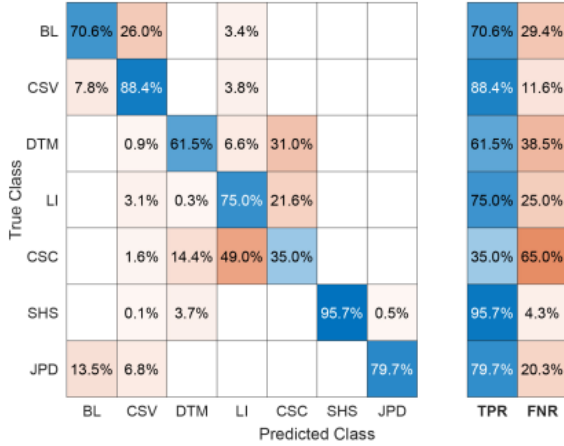


Figure 8. In flight data – no additional sensors: TPR vs FNR

The next case to be considered is that of the SVM trained on in-flight data with the addition of both a differential pressure sensor between the two actuator’s chambers and an LVDT transducer to measure the servovalve spool position.

As observable in Figures 11 and 12, results shows a significant improvement with respect to the in-flight data/no additional sensor case, achieving a total accuracy score of 87.2%. The main responsible for such improvement is the addition of the servovalve gain feature (A1), which is particularly effective for the disambiguation of faults occurring within the servovalve itself. The identification of the torque motor degradations exhibits a marked improvement thanks to this addition, achieving a TPR= 98.8 %.

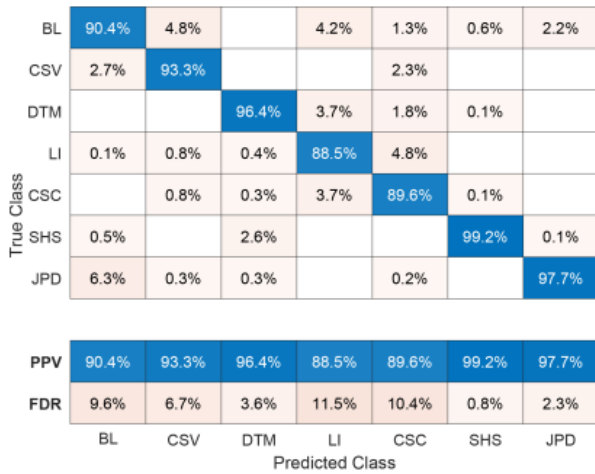


Figure 9. In-flight and pre-flight data – no additional sensors: PPV vs FDR

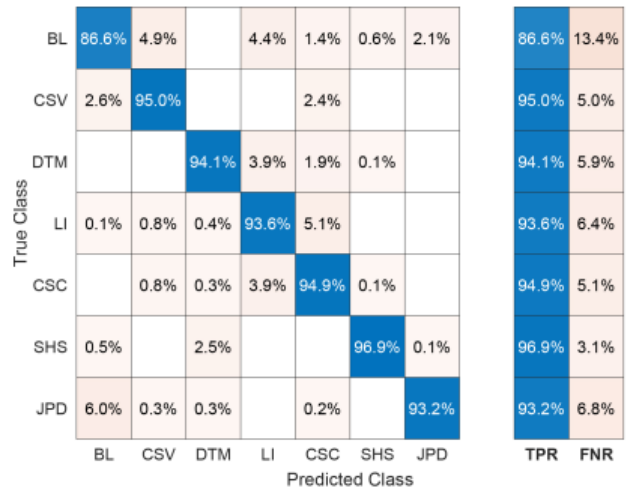


Figure 10. In-flight and pre-flight data – no additional sensors: TPR vs FNR

The classification of internal leakages also shows a significant improvement, with a TPR rising up to 90 %. Misclassification issues between the two considered failure modes within the actuator remains and, therefore, the worst SVM performances can be observed for the crack in the recentering spring (TPR=65.1 %). This is contrary to the evidence provided in (Autin et al., 2020), and a direct consequence of the SCAS operating conditions (almost negligible external load). Such observations suggest the need to include dedicated ground checks to effectively distinguish between the considered actuator faults.

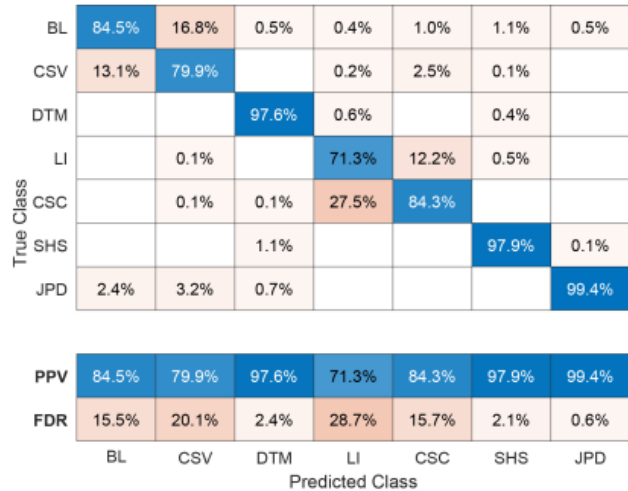


Figure 11. In-flight data – additional sensors: PPV vs FDR

| | | | | | | | | | | |
|------------|-----|-----------------|-------|-------|-------|-------|-------|------|-------|-------|
| True Class | BL | 78.6% | 18.0% | 0.5% | 0.5% | 0.8% | 1.1% | 0.5% | 78.6% | 21.4% |
| | CSV | 12.2% | 85.6% | | 0.2% | 1.9% | 0.1% | | 85.6% | 14.4% |
| | DTM | | | 98.8% | 0.8% | | 0.4% | | 98.8% | 1.2% |
| | LI | 0.1% | | | 90.0% | 9.4% | 0.5% | | 90.0% | 10.0% |
| | CSC | 0.1% | 0.1% | | 34.7% | 65.1% | | | 65.1% | 34.9% |
| | SHS | | | 1.1% | | | 98.8% | 0.1% | 98.8% | 1.2% |
| | JPD | 2.2% | 3.4% | 0.7% | | | | | 93.7% | 6.3% |
| | | | BL | CSV | DTM | LI | CSC | SHS | JPD | TPR |
| | | Predicted Class | | | | | | | | |

Figure 12. In-flight data – additional sensors: TPR vs FNR

The last considered case, which performances are provided in the confusion matrixes in Figures 13 and 14, sees the combination of in-flight data and on-ground checks in presence of dedicated sensors. As expected, the SVM achieve the highest accuracy score between the alternatives, reaching a value of 98.6 %. Although in practice lower performances can be expected, the results underline how the addition of sensors, together with short dedicated pre-flight checks can allow a robust classification process of all the seven damages considered.

6. PROGNOSIS

Prognosis is achieved through a Bayesian estimation method using a particle filtering approach as firstly proposed by (Orchard & Vachtsevanos, 2009).

| | | | | | | | | | |
|------------|-----|-----------------|-------|--------|-------|-------|-------|-------|-------|
| True Class | BL | 98.9% | 1.6% | | 0.6% | 0.3% | 1.0% | | |
| | CSV | 0.9% | 97.0% | | | 0.1% | 0.1% | | |
| | DTM | | | 100.0% | 0.1% | | 0.1% | | |
| | LI | 0.1% | | | 97.0% | | 0.3% | | |
| | CSC | 0.7% | | | | 99.6% | | 0.3% | |
| | SHS | | | | 2.3% | | 98.5% | | |
| | JPD | 0.2% | 0.7% | | | | | | 99.7% |
| | | | BL | CSV | DTM | LI | CSC | SHS | JPD |
| | | Predicted Class | | | | | | | |
| | PPV | 98.9% | 97.0% | 100.0% | 97.0% | 99.6% | 98.5% | 99.7% | |
| | FDR | 1.1% | 3.0% | | 3.0% | 0.4% | 1.5% | 0.3% | |

Figure 13. In-flight and pre-flight data – additional sensors: PPV vs FDR

| | | | | | | | | | | |
|------------|-----|-----------------|-------|-------|-------|-------|-------|------|-------|------|
| True Class | BL | 96.5% | 1.6% | | 0.6% | 0.3% | 1.0% | | 96.5% | 3.5% |
| | CSV | 0.9% | 98.9% | | | 0.1% | 0.1% | | 98.9% | 1.1% |
| | DTM | | | 99.8% | 0.1% | | 0.1% | | 99.8% | 0.2% |
| | LI | 0.1% | | | 99.6% | | 0.3% | | 99.6% | 0.4% |
| | CSC | 0.7% | | | | 99.0% | | 0.3% | 99.0% | 1.0% |
| | SHS | | | | 2.4% | | 97.6% | | 97.6% | 2.4% |
| | JPD | 0.2% | 0.7% | | | | | | 99.1% | 0.9% |
| | | | BL | CSV | DTM | LI | CSC | SHS | JPD | TPR |
| | | Predicted Class | | | | | | | | |

Figure 14. In-flight and pre-flight data – additional sensors: TPR vs FNR

This method takes advantage of a nonlinear process (fault / degradation) model to describe the expected dynamics of the fault progression and a measure model derived from the feature/wear progression dependence observed during the feature selection phase.

Prognosis through particle filtering is achieved by performing two sequential steps, prediction and filtering. Prediction uses both the knowledge of the previous state estimate and the process model to generate the a priori estimate of the state probability density functions (pdfs) for the next time instant,

$$p(x_{0:t}|y_{1:t-1}) = \int p(x_t|y_{t-1})p(x_{0:t-1}|y_{1:t-1}) dx_{0:t-1} \tag{4}$$

This expression usually does not have an analytical solution, requiring Sequential Monte Carlo algorithms to be solved in real-time with efficient sampling strategies (Roemer et al., 2011). Particle filtering approximates the state pdf using samples or “particles” having associated discrete probability masses (often called “weights”),

$$p(x_t|y_{1:t}) \approx \tilde{w}_t(x_{0:t}^i)\delta(x_{0:t} - x_{0:t}^i)dx_{0:t-1} \tag{5}$$

where $x_{0:t}^i$ is the state trajectory and $y_{1:t}$ are the measurements up to time t. The simplest implementation of this algorithm, the Sequential Importance Re-sampling (SIR) particle filter (Arulampalam et al., 2009), updates the weights using the likelihood of y_t as:

$$w_t = w_{t-1}p(y_t|x_t) \tag{6}$$

Although this traditional particle filtering technique has limitations, in particular with regards to the description of the distributions tails, and more advanced resampling schemes have been proposed (Acuña & Orchard, 2017), this technique was still deemed valid for a purely preliminary analysis. Long-term prediction of the fault evolution can be obtained by iterating the “prediction” stage, and are used to estimate

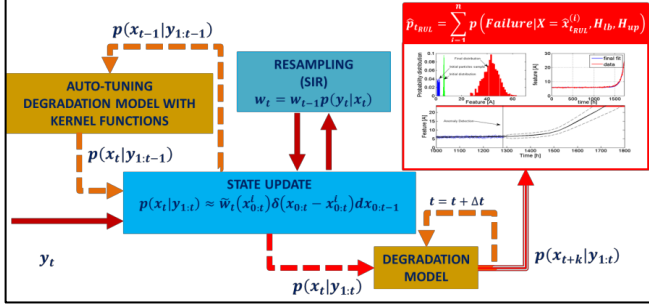


Figure 15. Prognostic routine.

the probability of failure in a system given a hazard zone that is defined via a probability density function with lower and upper bounds for the domain of the random variable, denoted as H_{lb} and H_{up} , respectively. Given the probability of failure, the RUL distribution for any given prediction can be computed along with the risk function (Acuña & Orchard, 2018).

The algorithm adopted for this paper follows the scheme provided in in Figure 9 (De Martin, Jacazio, et al., 2018); this approach makes use of degradation models that are tuned or their parameters adjusted through Recursive Least Square (RLS) algorithm embedded in the main routine, to compute the current a priori state of the system, $p(x_t|y_{1:t-1})$, and to perform the iterative calculation that leads to the long term prediction $p(x_{t+k}|y_{1:t})$. Auto-tuned models are required to describe and follow changes in the degradation process and to describe the process and measurement noise. The same algorithm is applied to each considered faults, although different settings are employed depending on the on-going degradation. The degradation models are simple time-variant functions depending on the expected evolution in time of the associated fault (polynomial, exponential and so forth). The prognostic algorithm is tested against simulated fault-to-

failure processes, where the severity of each fault mode (i.e. the crack progression in the recentering spring) evolves dynamically as a function of the system behavior and operating conditions (temperature, dynamic load, fluid pressure and so forth). The prognostic output is then evaluated according to the traditional metrics introduced by (Saxena et al., 2008), namely the Prognostic Horizon, evaluated as the first real RUL value for which the prognosis falls within a $\pm 20\%$ threshold of the real RUL, and the Relative Accuracy as defined as in Eq. (7).

$$RA = 1 - \frac{|RUL_r - RUL|}{RUL_r} \quad (7)$$

Results are summarized in Table 2, while an example of the prognostic output for the case of a slowly evolving short in the servovalve windings is provided in Figure 16. Prognostic analysis has been limited in this study to four failure modes. The inception and evolution of a crack within the feedback spring of the servovalve and within the recentering spring of the SCAS actuator have been modelled according to the crack propagation laws used in (Nesci et al., 2020). The occurrence of a short circuit condition in the servovalve windings has been modelled according to the Arrhenius Law, as suggested in (Gökdere et al., 2006). Finally, the internal leakage between the actuator's chambers is described as a combination of the effects of the wear of the sealing elements, itself following a modified Archard's law (Frölich et al., 2014). It can be noted that despite the improvement to the classification routine due to the introduction of additional sensors, results concerning the internal leakage of the SCAS actuator remain suboptimal. This can be traced down to the peculiar operating field of the SCAS actuators; since the actuation system is subjected to low external loads, the occurrence of internal leakage provides only subtle variations of the system performances,

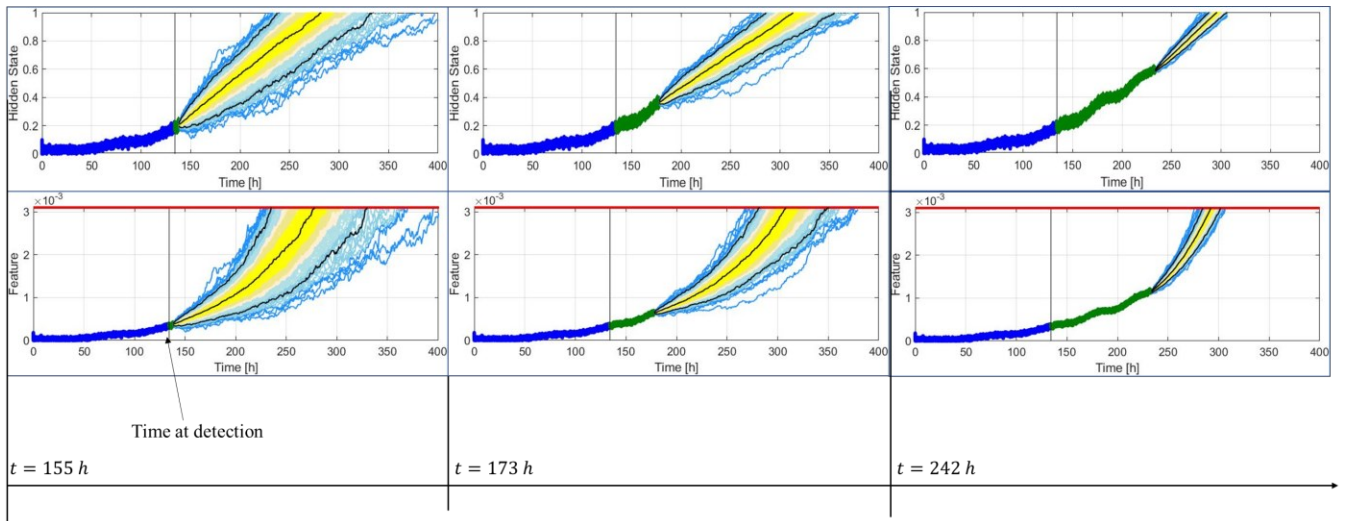


Figure 16. Prognosis of a slowly evolving short in the servovalve windings at different time instant

Table 2. Prognostic performance against simulated data-set

| Fault | Prognostic Horizon [h] | Average Relative Accuracy [%] |
|------------------------------------|------------------------|-------------------------------|
| Servo valve: winding short circuit | 182 hours | 87% |
| Servo valve: feedback spring crack | 140 hours | 82% |
| Actuator: internal leakage | 40 hours | 67% |
| Actuator: recentering spring crack | 170 hours | 83% |

which becomes evident only when the flow lost due to the leakage becomes a significant percentage of the maximum flowrate required during in-flight operations. During the fault diagnosis phase, such difficulties can be partially overcome using dedicated on-ground, pre-flight tests, in particular when stressing the actuator with high-speed commands. Such pre-flight checks provide however a low number of data-points, which makes this solution unfeasible for prognosis.

7. CONCLUSIONS

This paper deals with the preliminary evaluation of a PHM scheme for electro-hydraulic SCAS flight control actuators employed in rotary-wing vehicles. Traditionally these systems are equipped with a low number of sensors. Such conditions, together with the peculiar operating conditions of such actuators, can complicate the feature extraction and the fault diagnosis process. To overcome this issue, the introduction of dedicated sensors is considered, along the possibility to combine in-flight data with dedicated pre-flight checks to improve the fault classification performances. Results on simulated data-sets are encouraging. Although the best results are, as expected, obtained with the introduction of additional sensors, simulations suggest that good classification performances can be obtained even without additional transducers by considering both in-flight data and dedicated pre-flight checks. It is worth noting that, although promising, and despite relying on well-established simulation models, the results provided in this paper need proper experimental verification.

REFERENCES

- Acuña, D. E., & Orchard, M. E. (2017). Particle-filtering-based failure prognosis via sigma-points: Application to Lithium-Ion battery State-of-Charge monitoring. *Mechanical Systems and Signal Processing*. <https://doi.org/10.1016/j.ymssp.2016.08.029>
- Acuña, D. E., & Orchard, M. E. (2018). A theoretically rigorous approach to failure prognosis. *Proceedings of the 10th Annual Conference of the Prognostics and Health Management Society 2018 (PHM18), Philadelphia, PA, September 24-27*.
- Anguita, D., Ghelardoni, L., Ghio, A., Oneto, L., & Ridella, S. (2012). The ‘K’ in K-fold Cross Validation. *ESANN 2012 Proceedings, European Symposium on Artificial Neural Networks, Computational Intelligence and Machine Learning.*, April, 25–27.
- Arulampalam, M. S., Maskell, S., Gordon, N., & Clapp, T. (2009). A Tutorial on Particle Filters for Online Nonlinear/NonGaussian Bayesian Tracking. In *Bayesian Bounds for Parameter Estimation and Nonlinear Filtering/Tracking*. IEEE. <https://doi.org/10.1109/9780470544198.ch73>
- Autin, S., De Martin, A., Jacazio, G., Socheleau, J., & Vachtsevanos, G. (2020). Results of a Feasibility Study of a Prognostic System for Electro-Hydraulic Flight Control Actuators. *International Journal of Prognostics and Health Management*.
- Autin, S., Socheleau, J., Dellacasa, A., De Martin, A., Jacazio, G., & Vachtsevanos, G. (2018). Feasibility Study of a PHM System for Electro-hydraulic Servo-actuators for Primary Flight Controls. *Annual Conference of the Prognostic and Health Management Society, PHM 2018, Philadelphia, PA, September 24-27*, 1–19.
- Bertolino, A. C., De Martin, A., Jacazio, G., & Sorli, M. (2021). A case study on the detection and prognosis of internal leakages in electro-hydraulic flight control actuators. *Actuators*, 10(9). <https://doi.org/10.3390/act10090215>
- Byington, C. S., Watson, M., & Edwards, D. (2004). Data-driven neural network methodology to remaining life predictions for aircraft actuator components. *IEEE Aerospace Conference Proceedings*, 6, 3581–3589. <https://doi.org/10.1109/AERO.2004.1368175>
- Chen, Y., Mo, Z., Xie, L., & Miao, Q. (2019). Fault Detection and Diagnosis of Aircraft Electro Hydrostatic Actuator Control System. *Proceedings - 2018 Prognostics and System Health Management Conference, PHM-Chongqing 2018, Chongqing, China, October 26-28*. <https://doi.org/10.1109/PHM-Chongqing.2018.00172>
- De Martin, A., Dellacasa, A., Jacazio, G., & Sorli, M. (2018). High-Fidelity Model of Electro-Hydraulic Actuators for Primary Flight Control Systems. *BATH/ASME 2018 Symposium on Fluid Power and Motion Control*, V001T01A058--V001T01A058.
- De Martin, A., Jacazio, G., & Sorli, M. (2018). Enhanced Particle Filter framework for improved prognosis of electro-mechanical flight controls actuators. *PHM*

Society European Conference, PHME 2018, Utrecht, Netherlands, July 3-6, 4(1).

- De Martin, A., Jacazio, G., & Sorli, M. (2020). Preliminary Study towards the Definition of a PHM Framework for the Hydraulic System of a Fly-by-wire Helicopter. *Annual Conference of the Prognostics and Health Management Society*, 1–13.
- De Martin, A., Jacazio, G., Sorli, M., & Vitrani, G. (2021). A SIMULATION SURVEY ON THE EFFECTS OF PROGRESSING FAULTS WITHIN THE SCAS OF A FLIGHT CONTROL ACTUATOR FOR HELICOPTERS. *Proceedings of ASME/BATH 2021 Symposium on Fluid Power and Motion Control, FPMC 2021*, 1–9. <https://doi.org/10.1115/FPMC2021-69755>
- Frölich, D., Magyar, B., & Sauer, B. (2014). A comprehensive model of wear, friction and contact temperature in radial shaft seals. *Wear*, *311*(1–2), 71–80. <https://doi.org/10.1016/j.wear.2013.12.030>
- Gökdere, L. U., Bogdanov, A., Chiu, S. L., Keller, K. J., & Vian, J. (2006). Adaptive control of actuator lifetime. *IEEE Aerospace Conference Proceedings, 2006*. <https://doi.org/10.1109/aero.2006.1656096>
- Guo, R., & Sui, J. (2019). Remaining Useful Life Prognostics for the Electro-Hydraulic Servo Actuator Using Hellinger Distance-Based Particle Filter. *IEEE Transactions on Instrumentation and Measurement*. <https://doi.org/10.1109/tim.2019.2910919>
- Nesci, A., De Martin, A., Jacazio, G., & Sorli, M. (2020). Detection and Prognosis of Propagating Faults in Flight Control Actuators for Helicopters. *Aerospace*, *7*(3), 20. <https://doi.org/10.3390/aerospace7030020>
- Nunes, A. S., Daniel, L., Hage-hassan, M., & Domenjoud, M. (2020). Journal of Magnetism and Magnetic Materials Modeling of the magnetic behavior of permanent magnets including ageing effects. *Journal of Magnetism and Magnetic Materials*, *512*(December 2019), 166930. <https://doi.org/10.1016/j.jmmm.2020.166930>
- Orchard, M. E., & Vachtsevanos, G. J. (2009). A particle-filtering approach for on-line fault diagnosis and failure prognosis. *Transactions of the Institute of Measurement and Control*. <https://doi.org/10.1177/0142331208092026>
- Roemer, M. J., Byington, C. S., Kacprzynski, G. J., Vachtsevanos, G., & Goebel, K. (2011). Prognostics. In *System Health Management: With Aerospace Applications*. <https://doi.org/10.1002/9781119994053.ch17>
- Saxena, A., Celaya, J., Balaban, E., Goebel, K., Saha, B., Saha, S., & Schwabacher, M. (2008). Metrics for evaluating performance of prognostic techniques. *2008 International Conference on Prognostics and Health Management*, 1–17. <https://doi.org/10.1109/PHM.2008.4711436>
- Stachowiak, G. W., & Batchelor, A. W. (2014). Engineering Tribology. In *Engineering Tribology: Fourth Edition*. Elsevier. <https://doi.org/10.1016/C2011-0-07515-4>
- Urata, E. (2007a). On the torque generated in a servo valve torque motor using permanent magnets. *Proceedings of the Institution of Mechanical Engineers, Part C: Journal of Mechanical Engineering Science*, *221*(5), 519–525. <https://doi.org/10.1243/0954406JMES584>
- Urata, E. (2007b). Influence of unequal air-gap thickness in servo valve torque motors. *Proceedings of the Institution of Mechanical Engineers, Part C: Journal of Mechanical Engineering Science*, *221*(11), 1287–1297. <https://doi.org/10.1243/09544062JMES709>
- Urata, E., & Suzuki, K. (2011). Stiffness of the elastic system in a servo-valve torque motor. *Proceedings of the Institution of Mechanical Engineers, Part C: Journal of Mechanical Engineering Science*, *225*(8), 1963–1972. <https://doi.org/10.1177/0954406211403072>
- Vachtsevanos, G., Lewis, F., Roemer, M., Hess, A., & Wu, B. (2006). Intelligent Fault Diagnosis and Prognosis for Engineering Systems. In *Intelligent Fault Diagnosis and Prognosis for Engineering Systems*. John Wiley & Sons, Inc. <https://doi.org/10.1002/9780470117842>